

## Simulation of the executive operation of an electromagnetic actuator of a current sensor under various power supply conditions

**Abstract.** In this article, the authors investigate the influence of power supply conditions (frequency, current value) on the behavior of an executive electromagnet that can work as a current sensor. Power supply parameters and types of materials used in the construction of the device affect losses in the device, which in turn affects the operating temperature and properties of the entire device. The authors present simulation results in the ANSYS environment.

**Streszczenie.** W artykule autorzy badają wpływ warunków zasilania (częstotliwości, wielkości prądu) na zachowanie wykonawczego elektromagnesu mogącego pracować jako sensor prądu. Parametry zasilania oraz rodzaje materiałów zastosowanych do konstrukcji urządzenia wpływają na straty w urządzeniu, a to wpływa na temperaturę pracy całego urządzenia. Autorzy przedstawiają wyniki symulacji w środowisku ANSYS (Symulacja działania wykonawczego siłownika elektromagnetycznego sensora prądu w różnych warunkach zasilania).

**Keywords:** electromagnet, heating, attractive force, sensor.

**Słowa kluczowe:** elektromagnes, nagrzewanie, siła przyciągania, sensor

### Introduction

An electromagnet is a device that has a very wide range of applications in electrical engineering. Simple formulas that describe its operation encourage its construction and creation of new solutions [8]. The attractive force exerted on the spring-loaded electromagnet keeper (armature) is described by the formula (1):

$$(1) \quad F = \frac{B^2 \cdot S}{2\mu_0}$$

where  $S$  is the cross-sectional area of the spring-loaded electromagnet keeper,  $\mu_0$  is the magnetic permeability and  $B$  is the magnetic induction described by formula (2):

$$(2) \quad B = \frac{N \cdot I \cdot \mu}{L}$$

where  $I$  is the electric current flowing through the electromagnet coil (Fig. 1),  $N$  is the number of turns of the electromagnet coil, and  $L$  is the average length of the magnetic flux path in the electromagnet core. The attractive force  $F$  exerted on the spring-loaded electromagnet keeper, after substituting formula (2) into (1), will be equal to (3)

$$(3) \quad F = \frac{\mu^2 \cdot N^2 \cdot I^2 \cdot S}{2\mu_0 \cdot L^2}$$

The study of such forces allows for the construction of, among others, current sensors in electrical devices [7]. The appearance of force as an effect of current flowing through the coil of an electromagnet suggests the possibility of torque in the case of an appropriate number of degrees of freedom in the device under consideration. In [8] it was shown that in the case of shift of the spring-loaded electromagnet keeper, there is a change in the amount of magnetic energy (co-energy) stored in the system, and thus the possibility of the keeper moving back, and in the case of an appropriate number of degrees of freedom (e.g. rotation), there is a possibility of a mechanical torque. Therefore, using a properly designed electromagnet, one can attempt to construct a simple electric motor powered by alternating current. In this article, the authors will not deal with the construction of motors. The presented formulas do not contain any information regarding the behaviour of the

electromagnet at different positions of its spring-loaded keeper. The position of this movable keeper strongly influences the energy reserve in the electromagnet, and therefore its attractive force or, in the case of using an electromagnet for actuators' structures, it influences the precision of the keeper's action on the electromagnet's magnetic circuit. A similar problem also occurs when the electromagnet windings heat up. Temperature has a significant effect on the resistance of the electromagnet coil winding, and thus on the magnitude of the current flowing through this winding. Taking into account formula (3), this current and thus the temperature have a significant effect on the attractive force of the electromagnet keeper, and consequently on the precision of the device's operation. At the critical point, the restoring force of the spring is greater than the electromagnet's lifting force, and consequently the movable electromagnet keeper is torn off from the electromagnet core. The study of the dependence of the detachment force of the current sensor's spring-loaded keeper on thermal conditions is the subject of research in this paper.

### Description of the analyzed object

Figure 1 depicts the idea of research on a simple electromagnetic system. The system under study consists of a magnetic circuit, which includes a movable keeper (armature), a spring to generate a restoring force that tears the keeper off, and a sensor control component, which consists of an electromagnet winding and an electromagnet keeper that simultaneously closes the magnetic circuit. Due to the need to enable the keeper to move, the design provides an air gap between the stationary electromagnet core and its keeper. In order to limit the movement of the keeper, it was attached to the substrate by an additional element that accumulates mechanical energy and simultaneously forces the keeper to move, i.e. a spring. The energy stored in the spring affects the keeper with a force  $F$ . The coil is powered by an alternating current source that forces the current  $I$  to flow through the coil.

The diagram (Fig. 1) shows the equivalent resistance of the electromagnet coil as a temperature-dependent element. Due to the current flowing through the coil and the heat losses associated, it heats up. The resistance  $R_0$  of the wire section used to construct the electromagnet coil is:

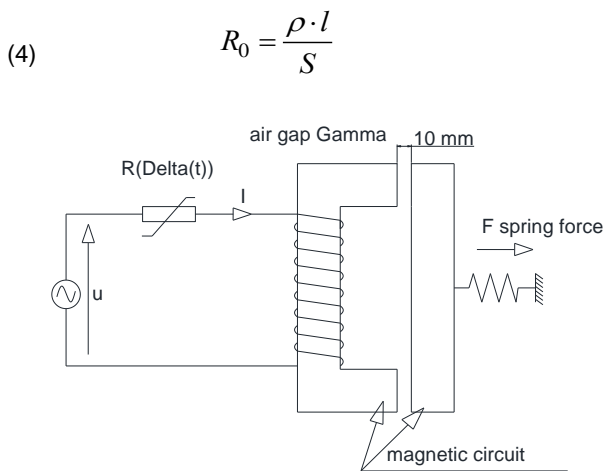


Fig. 1. Schematic diagram of the tested device

where  $\rho$  is the resistivity,  $l$  is the length of the wire and  $S$  is the cross-sectional area of the wire. The resistance of the wire used to construct the electromagnet coil will therefore be:

(5) 
$$R_D = R_0(1 + \alpha \cdot \Delta T)$$

The change in resistance with the changing temperature of the coil wire causes the change in the current flowing through the coil. This is a very important aspect of this change [7] because of the influence of the coil current on the force with which the magnetic field acts on the electromagnet keeper (3). The amount of these changes is described by formula (6):

(6) 
$$I = \frac{u}{R_D} = \frac{u}{\frac{\rho \cdot l}{S}(1 + \alpha \cdot \Delta T)}$$

where, for copper:

(7) 
$$\alpha_{CU} = 3,9 \cdot 10^{-3} \quad [K^{-1}]$$

The decreasing current has a significant impact on the attractive force of the keeper (3). In the case of sensor-type device construction, it can have a decisive influence on the device properties.

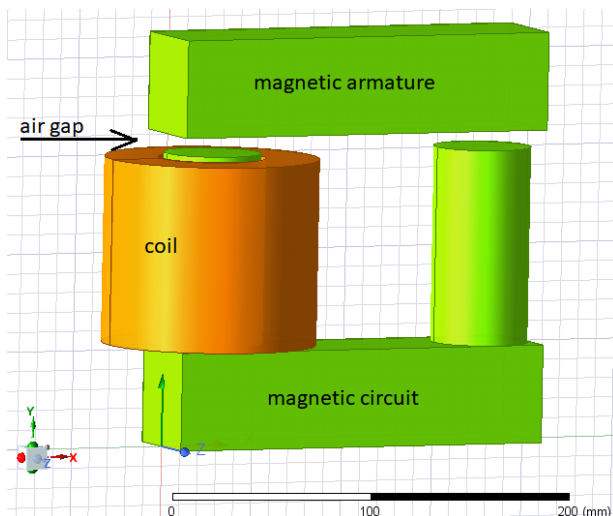


Fig. 2. Electromagnet model adopted for simulation

The shape of the electromagnet adopted for the project is shown in Figure 2. The sensor consists of an electromagnet with a movable keeper. This type of construction is used in many types of devices, e.g. [8]. Two forces act on the keeper. On the one hand, the keeper is attracted to the core due to the acting magnetic field of the coil, and on the other hand, the keeper is torn away from the core by the spring acting on it. Depending on the current value and the size of the air gap, the force acting on the keeper changes. The authors calculate the electromagnet force that attracts the armature to the core. The measurement of the force value can be a measure of the current flowing through the electromagnet coil.

Due to the requirements of the simulation program, the 3D dimensions were assumed proportional to the scale marked in the lower part of the electromagnet model drawing as a 100 mm section (Fig. 2).

### Numerical calculations and simulation of the object under analysis

Simulations were performed in the Ansys software environment [1, 2], while calculations of the magnetic field were performed in the Ansys Maxwell environment [3], in the part allowing for calculations of phenomena related to heat release in the model. The Ansys environment is software using the Finite Element Method and allows for calculations of phenomena occurring in devices and materials, related to the electromagnetic field theory, and thus allows for calculations of losses caused by eddy currents in objects. Calculation of the eddy current values indicates what losses, related to the current and material resistance, release heat in the object. The "Coupling" block structure allows for the conversion of data related to the current into information on the amount of heat released in the considered material. At the same time, these data can be used to present phenomena described by different equations in different environments. The above-mentioned structure allows to combine the calculation results of the "Maxwell" block (data concerning the magnetic field, where it occurs) with the calculation results of thermal phenomena of the "Icepak" block, i.e. phenomena described by equations of resistive and eddy current losses [3,4,5]. After calculations in the Maxwell environment and the "Coupling" block, one can start calculating the temperature distribution in the tested device. The Ansys Icepak program allows to use nonlinear thermal characteristic curves of materials used to construct the device. They can be used for both magnetic materials (magnetic circuits – iron) and electrical materials (electrical circuits – copper). Due to the nonlinearity of these characteristic curves, increasing the accuracy of calculations sometimes requires multiple repetitions of calculations in both blocks. The block diagram of this type of procedure is shown in the block diagram in Figure 3. This procedure is allowed by the Workbench block [5] and the system described in the documentation [1], called "Coupling" by the authors.



Fig. 3. Flowchart of calculations to increase their accuracy

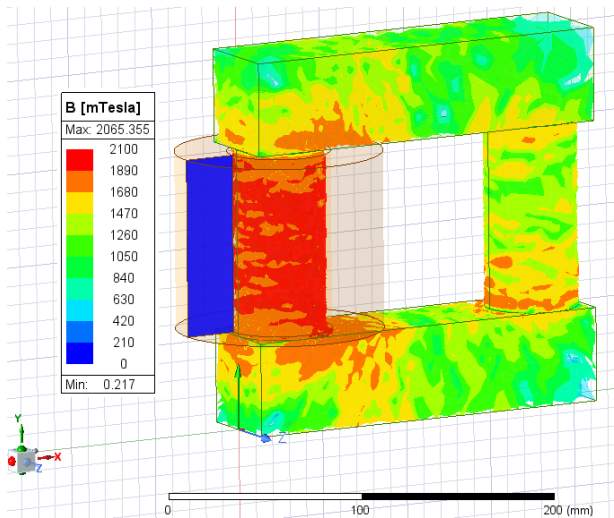


Fig. 4. Magnetic field distribution in the object's core (Ansys Maxwell)

The results of the first stage of calculations are presented in the form of the distribution of magnetic induction  $B$  in the core of the object. It can be seen that the largest amount of energy is accumulated in the area of the inner part of the control coil. High values of magnetic induction suggest large energy losses in the core, which, being surrounded by the coil, has a difficult process of dissipating this energy. Therefore, a precise analysis of the amount of heat released in this area of the core will be necessary.

The subsequent stages of the approximation of the electromagnetic loss assessment, which show, among other, the accuracy of the model, are presented in the table in Table 1.

The program provides for four successive stages of calculations. From the table, it can be seen that the results in the third and fourth stages are identical, which indicates that the calculation result has been stabilized and the assumed accuracy has been achieved.

Table 1. Subsequent electromagnetic loss estimates in four stages

	1. stage	2. stage	3. stage	4. stage
EM Loss	142.1 W	142.81 W	142.82 W	142.82 W

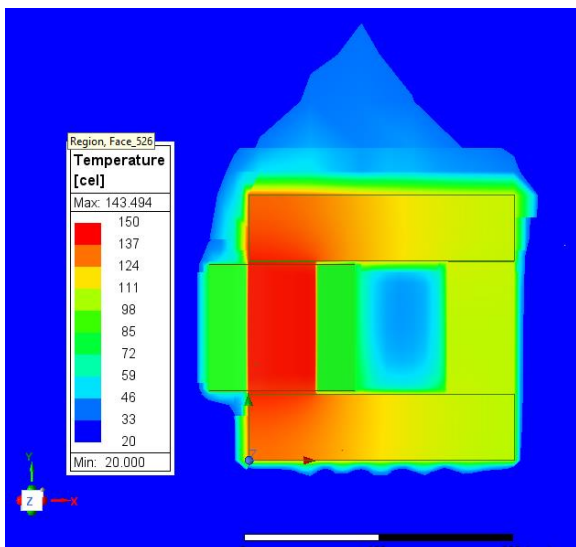


Fig. 5. Temperature distribution in the steel core of the tested object at a frequency of 50 Hz

The figure shows that the highest temperature will appear in the core in the area where the coil is placed. This is probably due to the coil hindering the core cooling process. This can cause the coil to overheat, which in turn

can damage it. "Ice Pack" allows for the analysis of the behavior of the object's surroundings, and consequently the changes that occur with changing operating conditions.

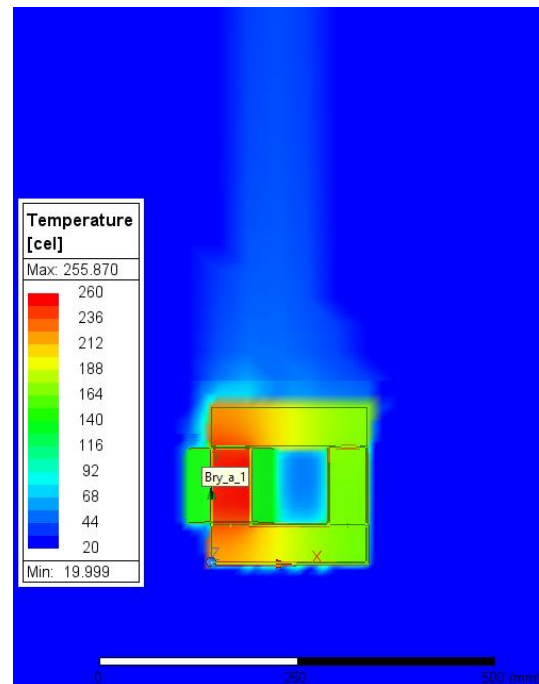


Fig. 6. Temperature distribution in the steel core of the tested object at a supply frequency of  $f=60\text{Hz}$ .

The table in Table 2. again shows the stabilization of the result after the fourth stage. However, increasing the frequency shows a significant increase in losses and core temperature. Due to the properties of the air surrounding the tested object, its movement occurs (vertical movement of warm air). This can cause heating of the elements in the vicinity of the tested object. The object temperature of  $255^{\circ}\text{C}$  can also cause them to ignite. The authors considered the effect of frequency on the simulated device to be equally interesting. Therefore, the device operation was simulated at a frequency of 200 Hz. As before, a four-stage simulation was performed to demonstrate the convergence of the calculations. The verification results are presented in the table in Table 3.

Table 2 The values of the subsequent estimates of electromagnetic losses in four stages, at the supply frequency  $f = 60\text{ Hz}$

	1. stage	2. stage	3. stage	4. stage
EM Loss	327.16 W	330.31 W	330.38 W	330.39 W

Table 3 The values of the subsequent estimates of electromagnetic losses in four stages, at the supply frequency  $f = 200\text{ Hz}$

	1. stage	2. stage	3. stage	4. stage
EM Loss	656.41 W	662.10 W	662.10 W	662.11 W

It can be seen that practically the second run is already stabilized with an accuracy of the second decimal place, and taking into account the size of losses calculated in the simulation, i.e. 662 W, this is an accuracy of the order of 0.0015%, so both the density of the calculation grid and the other parameters adopted in the program are sufficiently precise to assess the sought losses in the system. It can be seen that losses of this size, with the geometrical dimensions shown in Figure 4, cause a local increase in the object temperature to a value of  $426.2^{\circ}\text{C}$ .

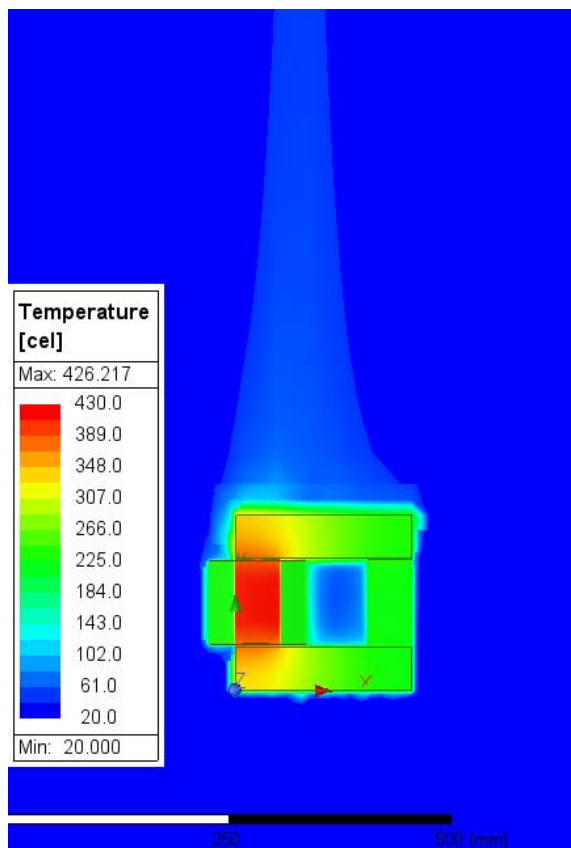


Fig. 7. Temperature distribution in the steel core and its surroundings at a frequency of 200 Hz

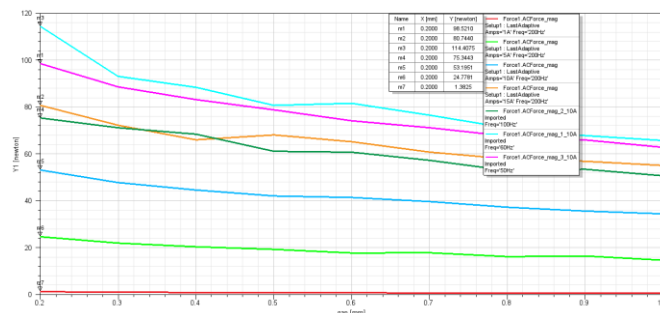


Fig. 8. Graph of the attractive force exerted on the object's magnetic keeper as a function of the distance between the keeper and the core

Increasing the supply frequency to 200 Hz completely changes all simulation results. The object temperature increases rapidly (according to Figure 7, locally to 426.2°C). The simulation results are presented in the form of a graph in Figure 8. The Table 4. is an additional explanation of the graph from Figure 8, allowing for a more precise description of the simulation results.

Simulations were performed in terms of various parameters as given in the table, changing the current in the coil and the frequency of the coil supply. With such selected parameters, the attractive force exerted on the magnetic keeper was calculated. Using the "Coupling" program block and the "Icepak" environment, the temperature distributions appearing in such operating conditions were calculated. The Table 3. contains the sets of the parameters (current and frequency) and the attractive force for the air gap of 0.2 mm, assigned to the respective markers on the graph in Figure 8.

The Table 4 assumes an air gap width of 0.2 mm. The force values for other air gap values in the range of 0.2...1.0 mm can be read from the graph in Figure 8.

Table 4. The magnitude of the attractive force exerted on the magnetic keeper for different simulation parameters

No.	Coil current $I_c$ [A]	Frequency $F$ [Hz]	Air gap $D$ [mm]	Force $F$ [N]	Marker
1	1	200	0,2	1,38	M7
2	5	200	0,2	24,77	M6
3	10	200	0,2	53,19	M5
4	15	200	0,2	80,74	M2
5	10	100	0,2	75,34	M4
6	10	60	0,2	114,40	M3
7	10	50	0,2	98,52	M1

## Conclusions

Based on the simulation results, it can be concluded that increasing the coil supply frequency does not have a positive effect on the device properties. A small increase in the supply frequency causes an increase in the attractive force exerted on the magnetic keeper and this property should be taken into account when designing this type of device, operating as a current sensor. However, increasing the supply frequency simultaneously causes an increase in eddy current losses, and consequently a change in the thermal conditions of the device, a change in the value of the attractive force exerted on the magnetic keeper and, finally, the risk of overheating and destruction of the device. This constitutes a significant risk of improper operation of the sensor.

In summary, when designing this type of current sensor, it is necessary to carefully check the effect of changing the supply frequency on the device's behavior and to precisely select the design parameters (the wire diameter of the device's control coil winding and the parameters of the magnetic circuit, especially the thickness and material properties of the sheet electrical steel used to assembly the device's core).

After manufacturing the designed device, the authors intend to perform measurements to verify the simulation results.

## Gratitude expression

The authors would like to thank the Organizers of the Campus Service PIONIER operating in many academic centers in Poland, including the Częstochowa University of Technology. The calculations necessary for this article would not have been possible without the use of software available to academic teachers and students of our university.

**Authors:** dr hab. inż. Marek Lis, Politechnika Częstochowska, Wydział Elektryczny, marek.lis@pcz.pl., mgr inż. Michał Kobierski, Politechnika Częstochowska, Szkoła Doktorska, fireman666@o2.pl, dr inż. Marek Chmiel, Politechnika Częstochowska, Wydział Elektryczny, marek.chmiel@pcz.pl,

## REFERENCES

- [1] Ansys, *System coupling Tutorials*, Ansys documentation 2023
- [2] Halmann D., *Modelowanie Układów Elektromagnetycznych w środowisku Ansys (Ansys Electronics Desktop)*, Uniwersytet Morski w Gdyni, ISBN 978-83-7421-383-7
- [3] Maxwell 23.1 application User's Guide
- [4] Ansys 23.1 application User's Guide
- [5] WorkBench 23.1 application User's Guide
- [6] Czaja P., Pluta W., Właściwości magnetyczne rdzeni przekładników sumujących wyłączników różnicowoprądowych, *Przegląd Elektrotechniczny*, 12 (2019), 109-112
- [7] Czaja P., Influence of the design of a residual current device on its break time, *Energies*, 15 (2022), 9054